Bone 123 (2019) 48–55

Contents lists available at ScienceDirect

Bone

journal homepage: www.elsevier.com/locate/bone

Case Report

Bone matrix hypermineralization associated with low bone turnover in a case of Nasu-Hakola disease

Mohammad Shboul[a,b], Paul Roschger[c,*], Rudolf Ganger[d], Lefteris Paschalis[c], Stamatia Rokidi[c], Shahin Zandieh[e], Jana Behunova[f], Christian Muschitz[g], Astrid Fahrleitner-Pammer[h], Alvin Yu Jin Ng[i], Sumanty Tohari[i], Byrappa Venkatesh[i], Carine Bonnard[i], Bruno Reversade[j], Klaus Klaushofer[c], Ali Al Kaissi[c,d]

[a] Department of Medical Laboratory Sciences, Jordan University of Science and Technology, Irbid 22110, Jordan
[b] Institute of Medical Biology, Immunos, Singapore
[c] Ludwig Boltzmann Institute of Osteology at Hanusch Hospital of WGKK and AUVA Trauma Centre Meidling, 1st Med. Dept. Hanusch Hospital, Vienna, Austria
[d] Orthopedic Hospital of Speising, Pediatric Department, Vienna, Austria
[e] Institute of Radiology and Nuclear Medicine, Hanusch Hospital, Vienna, Austria
[f] Institute of Medical Genetics, Medical University of Vienna, Austria
[g] St. Vincent Hospital – Medical Department II, The VINFORCE Study Group, Academic Teaching Hospital of the Medical University of Vienna, Vienna, Austria
[h] Department of Endocrinology and Diabetology, UKIM, Medical University Graz, Austria
[i] Institute of Molecular and Cell Biology, A*STAR, Singapore, Singapore
[j] Institute of Medical Biology, A*STAR, Singapore, Singapore

ARTICLE INFO

Keywords:
Nasu-Hakola disease
TYROBP gene
Bone mineralization density distribution (BMDD)
Osteoclasts
Transiliac bone biopsy

ABSTRACT

Analysis of tissue from a 34-years-old male patient from Austrian origin with a history of multiple fractures associated with painful episodes over the carpal, tarsal and at the end of the long bones respectively is presented. Radiographic images and axial 3DCT scans showed widespread defects in trabecular bone architecture and ill-defined cortices over these skeletal sites in the form of discrete cystic-like lesions. Family history indicated two sisters (one half and one full biological sisters) also with a history of fractures. Whole exome sequencing revealed two heterozygous missense mutations in *TYROBP* (MIM 604142; NM_003332.3) gene encoding for a cell-surface adaptor protein, which is part of a signaling complex triggering activation of immune responses. It is expressed in cells of the ectoderm cell linage such as NK and dendritic cells, macrophages, monocytes, myeloid cells, microglia cells and osteoclasts. The phenotype and genotype of the patient were consistent with the diagnosis of Nasu-Hakola disease (NHD) (OMIM 221770). Investigations at the bone material level of a transiliac bone biopsy sample from the patient using polarized light microscopy and backscatter electron imaging revealed disordered lamellar collagen fibril arrangement and extensively increased matrix mineralization. These findings are the first bone material data in a patient with NHD and point toward an osteoclast defect involvement in this genetic condition.

1. Introduction

Nasu-Hakola disease (NHD) also known as polycystic lipomembranous osteodysplasia with sclerosing leukoencenphalopathy (PLOSL; OMIM 221770) was first described by Nasu et al. [1,2] in Japan and Hakola et al. in Finland [3]. It is a rare (1 per 1.000.000) autosomal recessive disease characterized by abnormality of the neurological system, early dementia and personality changes in middle life accompanied by abnormalities in bone and adipose tissue. The condition manifests initially during early adulthood with swelling of the feet and ankles, which may be followed by fractures. Radiological evidence of cystic absorption of the bones is commonly observed. Pathological examination reveals membranocystic changes of the fat cells in the bone marrow and adipose tissue, and demyelination (sparing of the U-fibers) with gliosis and numerous axonal spheroids in the cerebral white matter. At the onset, learning difficulties have been described, which later evolved into dementia [4]. Paloneva et al. demonstrated loss of function mutations in the *TYROBP* gene (*DAP12*) encoding for a cell-surface adaptor protein in 19q13 linked families [5]. They also demonstrated mutations in the *TREM2* gene in families linked to 6p21-

* Corresponding author at: Ludwig Boltzmann Institute of Osteology, AUVA Trauma Center Meidling, Kundratstr. 37, A-1120 Vienna, Austria.
E-mail address: paul.roschger@osteologie.at (P. Roschger).

https://doi.org/10.1016/j.bone.2018.10.008
Received 29 August 2018; Received in revised form 5 October 2018; Accepted 8 October 2018
Available online 11 October 2018
8756-3282/

p22 rather than 19q13 [6]. TREM2 forms a receptor signaling complex with TYROBP and triggers activation of the immune responses in macrophages and dendritic cells. The two genes involved, encode different subunits of the same receptor signaling complex and thus both seem to be equally causative for NHD.

In the present study, we describe a patient with NHD displaying multiple cystic-like bone lesions. We performed a transiliac bone biopsy for histo-pathological examination and to investigate a potential impact of the *TYROBP* gene mutation on the material quality of the bone in this patient [7]. The diagnosis was mainly based on a whole exome sequence analysis, which revealed recessive or compound heterozygous mutations in the *TYROBP* gene confirmed by Sanger sequencing in the family. These mutations were compatible with the phenotype of NHD (see above). We report on lamellar collagen fibril arrangement, bone matrix mineralization density and collagen cross-linking by light microscopy, backscatter electron microscopy and Fourier transform infrared imaging, respectively.

2. Material and methods

2.1. Subject

This 34-year-old man with a history of multiple painful pathological fractures associated with minor traumas over the carpals, tarsals and at the ends of the long bones, respectively, which manifested after his 26th year. Family history indicated two sisters (one half and one full biological sisters) both with a history of fractures exclusively during their first decade of life. The parents manifested tarsal fractures in their early lives. But, grandparents and relatives from both maternal and paternal sides had a history of early dementia. There was no consanguinity in this family, but the family lives in a certain geographical area for generations and all their ancestors are of Austrian origins. Radiographic examination of the patient revealed discrete cystic-like bone lesions in the carpals, tarsals and the metaphyses of the long bones (Fig. 1). Axial 3D-CT scans showed widespread defects in mineralized bone architecture over the carpal, tarsal/metatarsal and the ends of the long bones associated with ill-defined cortices (Fig. 1). Skeletal scintigraphy detected focal osseous metabolic events in these sites of cystic-like bone lesions described above. Bone mineral density measurements by Dual Energy X-ray Absorptiometry (DXA) revealed increased density in the spine (L1-L4 T-score 2.7) and but normal density at the femoral neck (T-score 1.1). The patient was treated by us with a combination of vitamin B1, B6 and B12 to overcome frequent sense of fatigue and loss of memory. He received no bone specific treatment (like bisphosphonates, denosumab, teriparatide) with the exception of calcium (500 mg/day) and vitamin D (2.000 IU/day) supplementation. Otherwise, he was still in good athletic condition, muscular, with a height of 188 cm at the 90th percentile of normal, weight of 105 kg and head circumference 57.5 cm both were at the 75th percentile. Laboratory findings of the patient were non-contributory with no hormonal or mineral imbalance noted, apart from low normal 25-hydroxyvitamin D coupled with a mild increase in iron level, though ferritin levels were normal. He did not receive iron supplement. His alkaline phosphatase level was normal. Markers of bone formation and resorption (P1NP, CTX, iPTH, 25-hydroxyvitamin D, serum calcium and phosphate) fell within the lower normal range. A transiliac bone biopsy was performed for histopathological examinations. No tetracycline labeling has been performed. There were no radiological or skeletal scintigraphical signs that the iliac crest was affected by the disease. Our patient was genetically screened at first for osteogenesis imperfecta, but showed no mutations for *COL1A1-A2*. Subsequently, he was genetically tested for familial expansile osteolysis [8]. This genetic disease starts with metadiaphyseal osteolysis in the second decade, with progressive nature, painful and evolving into medullary expansion. The disease-causing gene is *TNFRSF11A* mapped on 18q22.1. However, these genetic tests for the patient were negative. The possibility of fibrogenesis imperfecta ossium characterized by osteoporosis and patchy rarefaction with subsequent fractures due to defective formation of the cone collagen

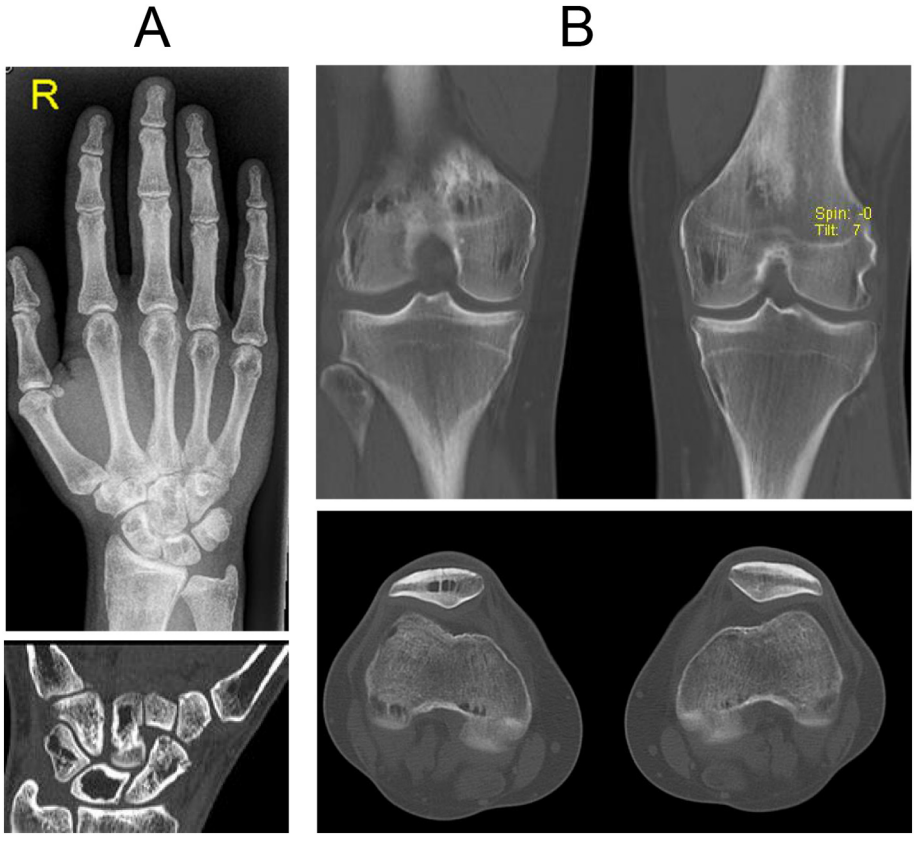

Fig. 1. a) top - AP radiograph of the right hand shows cystic rarefaction of the carpal bones associated with painful and restricted movement; bottom - 3D CT scan of the right hand confirms the cystic bone rarefaction along the carpal bones. b) 3D reformatted CT scan of the inferior femora shows bilateral massive cystic bone lesion and rarefaction in the epi-metaphyseal regions, whereas there is a single bone cyst over the metaphysis of the left tibia. Also the patella is affected.

fibers, was also excluded by clinical and radiographic phenotypic characterizations. Finally, whole exome sequencing was performed to reveal the underlying genetic defect.

2.2. Whole exome sequencing

Whole exome sequencing has been performed at the Human Genetics and Molecular Biology, Medical Laboratory Sciences, Faculty of Science, Institute of Molecular and Cell Biology, A*STAR, Singapore. One microgram of genomic DNA from each parents and the propositus was used for exome capture with Agilent Technologies SureSelectXT All Human ExonV6 Kit. DNA was sheared to achieve an average fragment size of 200 bp and amplified as per SureSelect protocol. The exome library was prepared on an Ion OneTouch System and sequenced on an Ion Proton instrument (Life Technologies, Carlsbad, CA, USA) using one Ion PI chip. Sequence reads were aligned to the human reference genome (Human GRCh37 (hg19) build) using Torrent Mapping Alignment Program (TMAP) from the Torrent Suite (v5.0.2). The variants were called using the Torrent Variant Caller (TVC) plugin (v5.0.2), and were annotated with the associated gene, location, quality-score, coverage, predicted functional consequences, protein position and amino acid changes, SIFT [30], PolyPhen2 [31], Granthan [32] and M-CAP [33] prediction scores, phyloP conservation scores [34] and 5000 genomes Minor Allele Frequencies Variants were filtered for common SNPs using the NCBI's "common and no known medical impacts" database (ftp://ftp.ncbi.nlm.nih.gov/pub/clinvar/vcf_GRCh37/) and the Exome Aggregate Consortium (ftp://ftp.broadinstitute.org/pub/ExAC_release/release0.2/). We then removed variants that were present in > 1% of the previously 545 sequenced samples. For the Trio analysis, 15.9 Gb, 15.2 Gb and 15.9 Gb were sequenced per sample with an average read length of 182 bp, 178 bp and 180 bp for the father, mother and affected son respectively. An average coverage of 172× (Father), 172× (Mother) and 185× (son) was achieved over the exome with 97% of the bases covered at least 20×. In this Trio, a total of 69,797 variants were identified across protein-coding exons, UTRs, splice sites and flanking introns. After applying all filters, a final set of 572 variants (18 homozygous, 92 heterozygous, 435 compound heterozygous and 27 X-linked homozygous) were identified.

2.3. Examinations of transiliac bone biopsy sample

The undecalcified transiliac bone biopsy was embedded in polymethylmethacrylate (PMMA) using standard procedures [9]. After earlier histopathological examinations of the bone sample at the Department of Endocrinology and Diabetology at Medical University Graz, further analyses were performed at the Ludwig Boltzmann Institute of Osteology in Vienna to elucidate whether the genetic defect has an impact at the tissue and material level of bone, using non-destructive spatially resolved physical methods, like polarized light microscopy, backscatter electron microscopy and Fourier transform infrared imaging. Longitudinal sections of the bone sample cylinder were obtained. Three µm thick sections were cut for bone histomorphometry and five µm thick sections for Fourier transform infrared imaging (FTIRI) analysis. The surface of the residual sample block was flattened by grinding and polishing (Logitech PM5, Glasgow, Scotland) to facilitate quantitative backscatter electron imaging (qBEI) analysis.

2.3.1. Histomorphometric assessments

The structural parameters were calculated based on binary images (mineralized bone area versus soft tissue area) as acquired by backscatter electron microscopy (Fig. 3). The assessment of static parameters of bone formation and resorption were done on Goldner's trichrome stained 3 µm thin sections by a light microscope (Axiophot, equipped with digital camera AxioCam HRc, Zeiss, Oberkochen, Germany). All bone parameter values were determined according to ASBMR guidelines [10] using custom image analysis routines on Image J (version 1.50f; NIH, Bethesda, MD, USA) [11] and compared with published reference data [12].

2.3.2. qBEI

The residual block sample was used for the analyses of bone matrix mineralization by qBEI as described elsewhere [13]. A scanning electron microscope equipped with a four quadrant semiconductor backscattered electron detector (Zeiss Supra 40, Oberkochen, Germany) was employed. The entire cross-sectioned bone sample area was imaged with a spatial resolution of 1.76 µm/pixel. The gray levels reflecting the calcium content were calibrated by the material contrast of pure Carbon and Aluminum so that the resulting gray level histograms could be transformed into calcium weight percent (wt% Ca) histograms designated as bone mineralization density distribution (BMDD) as described previously [14]. Five BMDD parameters were considered to characterize the BMDD: CaMean: the mean calcium concentration (weighted mean); CaPeak: the most frequently occurring calcium concentration in the sample (the peak position of the BMDD); CaWidth: the width of the BMDD distribution (full width at half maximum) reflecting the heterogeneity in matrix mineralization; CaLow: the percentage of low mineralized bone area, (below 17.68 wt% Calcium) normally representing bone areas undergoing primary mineralization; CaHigh: the percentage of highly/fully mineralized bone matrix, which has a calcium content above 25.30 wt% Ca (corresponding mainly to interstitial bone). The obtained data were compared against a previous published normative reference database [15].

2.3.3. FTIRI

In order to obtain information on the pyridinoline/divalent collagen crosslinks ratio, spatial distribution vibrational spectroscopic images of thin bone tissue sections (~5 µm) were obtained. A Bruker Equinox 55 (Bruker Optics) spectrometer interfaced to a 64 × 64 Mercury Cadmium Telluride (MCT) array detector, and equipped with a Hg fluorescence lamp (A674-HG, Bruker Optics) was employed [16–18]. Spectral resolution was 4 cm^{-1} (128 co-additions). Background spectra were collected under identical conditions from the same BaF_2 windows (without a section present) at the beginning and end of each experiment to ensure instrument stability. The spectrometer was continuously powered to minimize warm-up instabilities and purged with dry-air (Bruker Optics) to minimize the water vapor and CO_2 spectral contributions. After acquisition, spectra were zero-corrected for the baseline in the spectral area of Amide *I* & II (~1490–1700 cm − 1) and water vapor and PMMA spectral interferences corrected for as previously described [16], followed by calculation of the absorbance ratio at 1660 and 1690 cm^{-1}. This ratio has previously been shown to correspond to the relative ratio of pyridinoline and divalent collagen crosslinks, due to the perturbation that the cross-links exert on the molecular vibrations of the carbonyl groups present in the collagen chains [19–21].

2.4. Statistical analyses

All outcomes (BMD, histomorphometric parameters, BMDD) have been measured once in a single patient. Thus, the degree of deviations of patient's outcomes from normative reference mean data are given in units of SD (T-scores or *Z*-scores) of the reference values.

3. Results

3.1. Mutations in the TYROBP gene

In the exome sequencing analysis, a final set of 572 variants (18 homozygous, 92 heterozygous, 435 compound heterozygous and 27 X-linked homozygous) were found. Among them, two heterozygous missense mutations in *TYROBP* gene (MIM 604142; NM_003332.3) in trans-allelic configuration were detected: c.94G > A; p.Asp32Asn

Table 1
Phenotype and genotype in propositus with NHD and his four family members.

Patient	First presentation	Radiographic phenotype	Neurological manifestations	Genotype
Propositus (male)	10 yrs-tarsal fractures	CT scan: cystic like osteolytic lesions in talus and calcaneus	Euphoria, memory losses Cerebral MRI: hyperintensities in periventricular white matter	c.94G > A/c.167T > C[a]
Mother	Kyphosis	Osteoporosis	Dementia	N/c.167T > C
Father	Kyphosis	Osteoporosis	Dementia	N/c.94G > A
Sister	12 yrs-Tarsal Fractures	Osteolytic lesions talus and calcaneus	No neurological symptoms	N/c.167 T > C
Half sister	9 yrs-tarsal fractures	Osteolytic lesions talus and calcaneus	No neurological symptoms	N/c.94G > A

N: indicates that this member is heterozygous normal for one of the mutations.
[a] Compound heterozygous missense mutations in *TYROBP* (MIM 604142; NM_003332.3) gene.

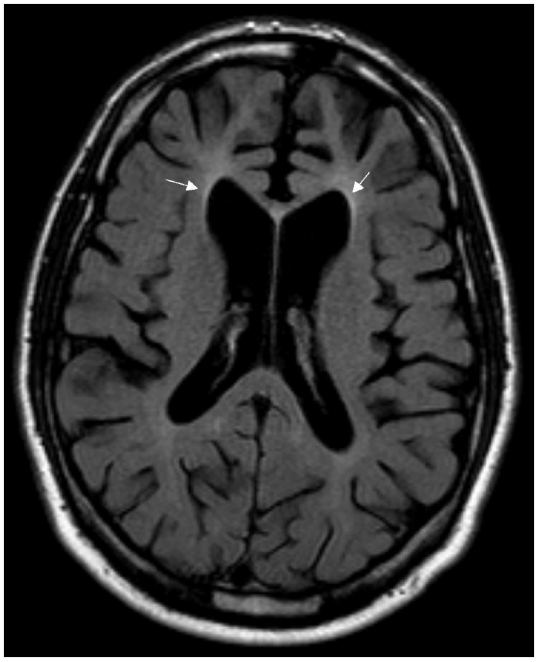

Fig. 2. Magnetic resonance image (MRI) of the brain from the propositus with Nasu-Hakola disease. Fluid-attenuated inversion recovery (FLAIR) sequence MRI showing periventricular leukoencephalopathy (white arrows).

(paternally inherited) and c.167 T > C; p.Leu56Pro (maternally inherited). Mutations of this gene are known to cause NHD (OMIM 221770) [4]. Sanger sequencing in all family members (Table. 1, Fig. 4) confirmed the presence of these mutations. As a consequence of the genetic findings, cerebral magnetic resonance tomography (MRT) was performed in the patient, detecting hyperintense signal changes in the periventriculars in connection with vascular leukoencephalopathy compatible with the genotype of NHD (Fig. 2). This periventricular white matter hyperintensity is known to increase the probability for cognitive impairment, progressing into dementia. This is the first time NDH diagnosed in Austria.

3.2. Low bone turnover and abnormal collagen fibril arrangement

The histomorphometric outcomes of the propositus (male, aged 32 years) was compared to those from the 31–40 years age range of the reference/control database of Rehman et al. (1994) [12] (Table 2, Fig. 3): i) The bone volume (BV/TV), the trabecular thickness (Tb.Th) and number of trabeculae (TB·N) of the propositus were within mean ± 1SD of the reference. The cortical width Ct.Wi (*Z*-score > 2) was markedly increased, while the cortical porosity was within the normal range. ii) The static parameters of bone formation showed reduced osteoid volume (OV/BV) (Z-score < −1), normal osteoid thickness (O·Th), and decreased osteoid surface OS/BS (Z-score < −1). Moreover, the osteoblast surface Ob.S/BS (Z-score < −3) was significantly diminished. iii) The static parameter of bone resorption showed a normal eroded bone surface (ES/BS) and a reduced osteoclast surface (Z-score < −5) and osteoclast number per tissue area, respectively (Table. 2). iv). The bone lamellar orientation within the cancellous compartment was partly disordered (Fig. 3E). Further, there were numerous areas of osteon formation within the trabecular bone (Fig. 3F).

Table 2
Bone histomorphometry of propositus.

Parameters	Propositus	Propositus *Z*-score	Control values [a] (31–40 years)
	Structural parameters		
BV/TV [%]	21.8	−0.1	22.0 ± 3.9
Tb.Th [μm]	160.3	0.5	148 ± 23
Tb.N [/mm]	1.4	−1.2	1.66 ± 0.22
Ct. Wi [mm]	1.9	2.7	1.15 ± 0.28
Ct.Po [%]	6.2	0.6	3.5 ± 4.6
	Static parameters of bone formation		
OV/BV [%]	1.2	−1.2	3.5 ± 1.9
O.Th [μm]	11.9	0.5	9.7 ± 4.6
OS/BS [%]	7.8	−1.3	14.0 ± 4.6
Ob.S/BS [%]	2.7	−3.0	6.0 ± 1.1
	Static parameters of bone resorption		
ES/BS [%]	4.1	−0.2	4.5 ± 1.9
Oc.S/BS [%]	0.08	−1.4	1.14 ± 0.74
N. Oc/ T.Ar [1/mm^2]	0.07	n.a.	4.3 [0.2–19]

n.a. no reference information available for calculation of patient's Z-score.
[a] Published values from Rehman et al. [12], mean ± SD, median [range].

3.3. Hypermineralization of the bone matrix

The entire biopsy sample surface was analyzed for bone matrix mineralization density in the cancellous and cortical compartments individually (Fig. 3). An example of qBEI image from trabecular bone as used for BMDD analysis is shown in Fig. 5a. The calculated BMDD curves of trabecular and cortical bone were shifted to the right, toward higher matrix mineralization compared to normative reference values (Fig. 5b). The measured BMDD parameter outcomes of cancellous and cortical bone including the T-scores of normative references are listed in Table. 3: i) Cancellous bone of the patient showed distinctly increased bone matrix mineralization (CaMean and CaPeak +6.5%, T-score > 3) as well as highly mineralized bone (CaHigh, + 372%, T-score > 6). ii) The heterogeneity of matrix mineralization (CaWidth, +8.7%) was close to T-score + 1. iii) The portion of lowly mineralized bone (CaLow, −36.7%, T-score < −1) was reduced. iv) The mean values of the two cortical BMDD-parameters are very similar to those of the cancellous compartment (Table. 3). This is in agreement with the findings in normal/healthy transiliac bone compartments of premenopausal women (age range 24–48 years), where the differences between cancellous and cortical BMDD parameters were found to be

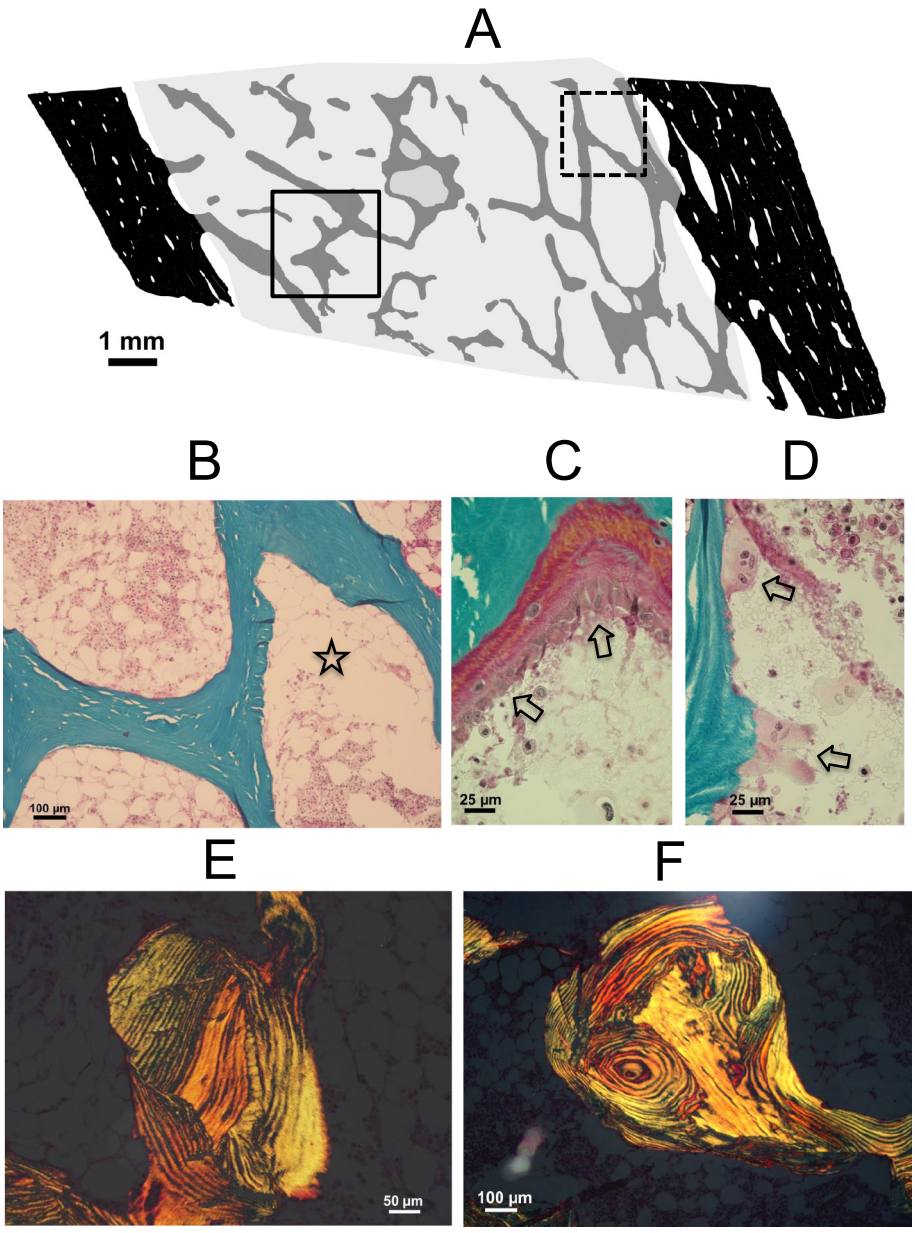

Fig. 3. Histological features of the transiliac bone biopsy sample: a) Binary image (mineralized bone area versus soft tissue area) of the sectioned bone area as derived from backscatter electron image (black: cortical area, dark gray: trabecular area). Solid black rectangle indicates trabecular detail shown as qBEI image in Fig. 3a. Dashed black rectangle indicates trabecular detail close to that analyzed by FTIRI shown in Fig. 3c. b) Typical trabecular bone feature lacking osteoid and bone cells. Note, area with abnormal large amount of fat cells in the bone marrow (star). c) The only bone-forming site found in the total bone area of the studied biopsy cross-section (seam of osteoid and osteoblasts, arrows). d) Examples of osteoclasts (arrows), remark: resorption lacunae are rather small. e–f) Polarized light image of trabecular features, showing abnormal lamellar orientation as well as unusually frequent and abrupt changes in bone lamellar orientation and intra trabecular osteon formation.

rather minor [22].

3.4. Normal collagen crosslinks ratio

The ratio of pyridinoline/divalent collagen cross-links (xlink) as measured by FTIRI did not deviate from that of normal bone, which was previously reported to be between 4 and 3 [23]. This is demonstrated by by xlink frequency histogram as deduced from the xlink map of a trabecular bone feature (Fig. 5c, d). The derived histogram parameters weighted mean xlink value ($xlink_{MEAN}$) and the most frequent measured xlink value ($xlink_{PEAK}$) were 3.314 and 3.419, respectively. The variation of the xlink values around the peak value as indicated by the full width at half maximum ($xlink_{WIDTH}$) was 0.36 Δ xlink.

4. Discussion

The clinical symptoms of NHD follow a characteristic progression with aging [4]. In a first latent stage from 0 to about 20 years, the development of the individuals and early life are unremarkable. This is followed by an osseous stage from 20 years on, which starts with pain and slight swelling in the ankles and feet, progressing into pathological fractures in the extremities. During this phase, radiological examination typically shows multiple bone cystic-like defects in metaphyseal and epiphyseal trabecular bone, predominantly in the upper and lower limb. Concomitantly to these skeletal abnormalities, an early neurological (32 to 52 yrs) followed by a late neurological stage (42 to 60 yrs) develops, which eventually results in profound dementia with corresponding changes in the brain tissue. Early death occurs during the fourth and fifth decade of life, due to respiratory or urinary infections.

Considering the focal cystic defects in the long bones in NHD, it is not surprising, that the transiliac bone biopsy sample of the patient did not reveal such trabecular defects or cystic-like lesions. On the other hand, we found that these mutations in the *TYROBP* gene seem to have an impact globally at the bone tissue/material level, in addition to the aforementioned local defects. Bone histomophometric analyses provided evidence for a distinct increase in cortical thickness and a reduction in bone formation and resorption. The lamellar arrangement of collagen fibrils in trabecular bone was partly disturbed and exhibited

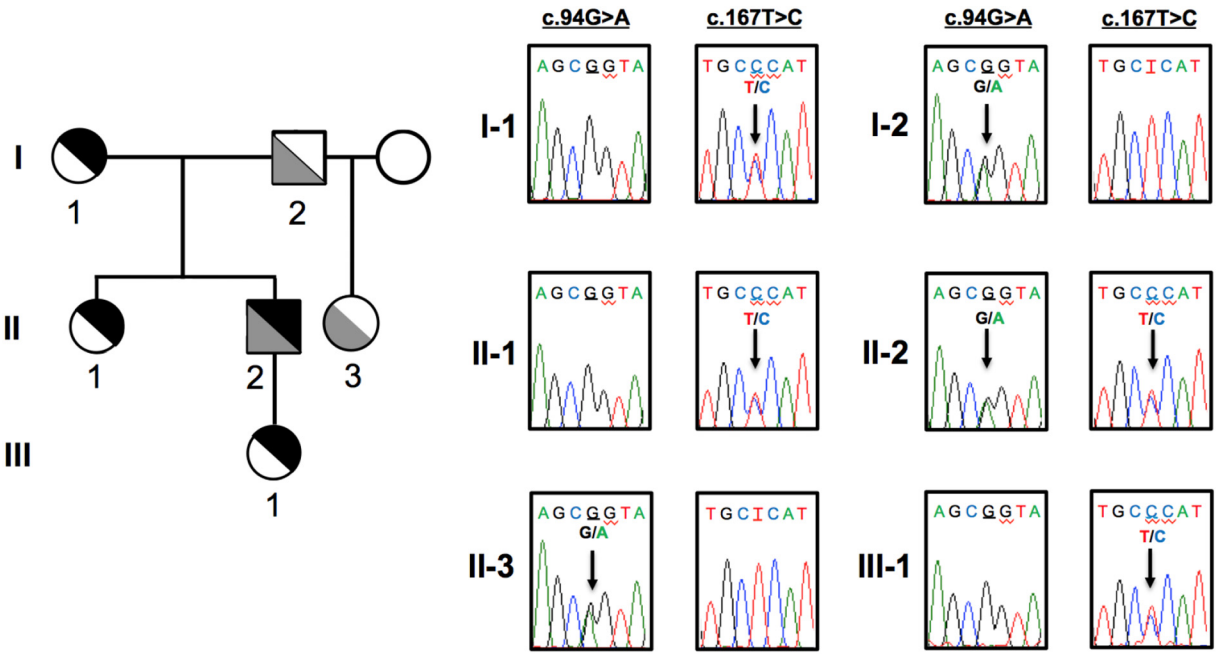

Fig. 4. Family pedigree of propositus carrying compound heterozygous missense mutations in the *TYROBP* gene.

abnormal changes in orientation. Furthermore, the bone matrix mineralization density was significantly increased, unlike the collagen crosslink pattern.

Little is known about the molecular mechanism leading to the complications observed in NHD. TYROBP is a cell-surface adaptor protein, which bears an immunoreceptor tyrosine-based activation motif (ITAM) in the cytoplasm domain [4]. Moreover, it seems that TREM2, a polypeptide that belongs to the immunoglobulin superfamily (Ig-SF), forms a receptor signaling complex with TYROBP, which triggers activation of the immune responses in macrophages and dendritic cells. It is known that mutations in *TREM2* gene alone can also induce the NHD [6]. TYROBP and TREM2 are reported to be associated with

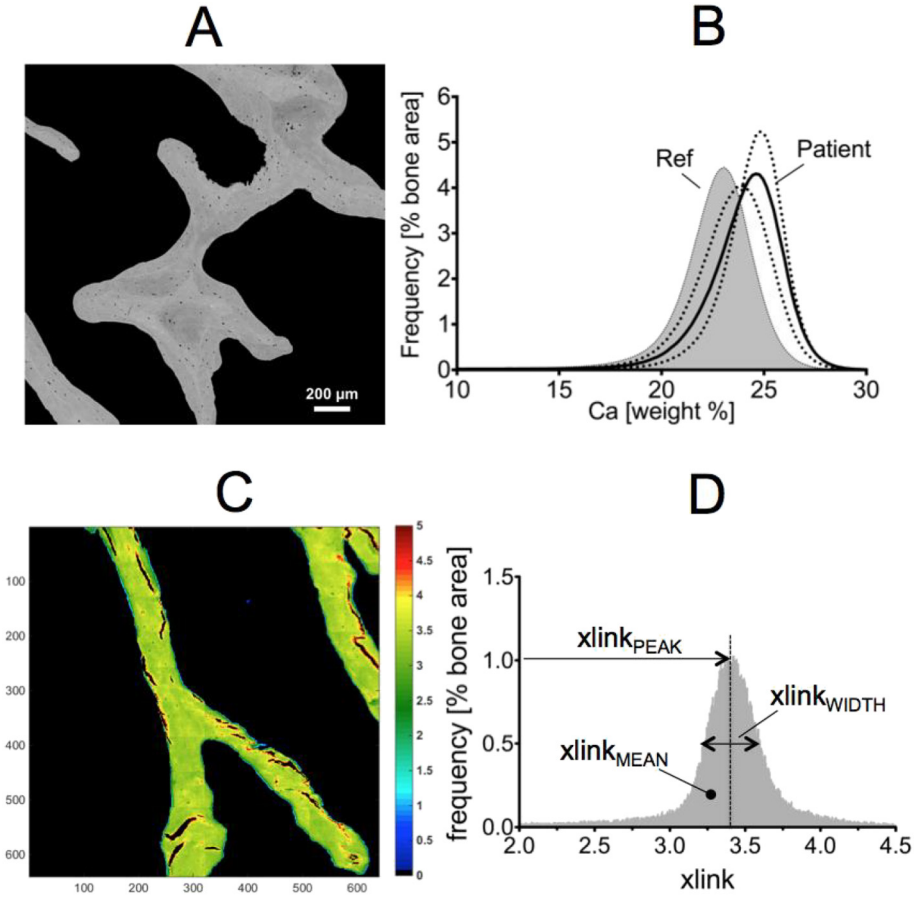

Fig. 5. a) Example of trabecular bone feature acquired by qBEI to determine BMDD. b) BMDDs derived from the total sectioned bone area as shown in Fig. 1a: solid line frame - trabecular BMDD, dotted line - cortical BMDDs of both cortical plates separately. Ref = adult trabecular reference BMDD [14]. c) FTIR mapping of cross-links ratios (xlink = absorbance ratio at 1660 and 1690 cm^{-1}) of a trabecular bone feature shown in Fig. 2a (dashed line frame). d) Corresponding histogram derived from FTIR image (C). The histogram parameters $xlink_{MEAN}$, $xlink_{PEAK}$, $xlink_{WIDTH}$, derived are indicated.

Table 3
BMDD parameters of propositus.

BMDD variables	Cancellous bone				Cortical bone[b]
	Propositus	%Diff vs Ref	T-score	Cn-Ad Ref [a]	Propositus
CaMean [wt% Ca]	23.65	+6.5	+3.2	22.20 ± 0.45	23.71
CaPeak [wt% Ca]	24.43	+6.5	+3.8	22.94 ± 0.39	24.26
CaWidth [Δwt% Ca]	3.64	+8.7	+0.9	3.35 ± 0.34	3.47
CaLow [%]	3.12	−36.7	−1.2	4.93 ± 1.57	2.20
CaHigh [%]	26.20	+372.1	+6.2	5.55 ± 3.32	23.72

[a] Cn-AdRef: previously published values of cancellous bone of adult healthy reference cohort, mean ± SD [13,15].
[b] Mean value of the two cortical plates.

several human and mouse receptors expressed in natural killer cells, macrophages, monocytes, myeloid cells, dendritic cells, in tissues like brain (microglia cells) and bone (osteoclasts) [4]. All of them belong to the ectodermal cell lineage. Thus, it is likely that NHD results from inactivation/disturbances of the TREM2/TYROBP signaling pathway. In the case of bone tissue, it may be speculated that osteoclastogenesis and/or osteoclast function might be affected by a dysfunction of this signaling pathway.

Indeed, a mouse model of DAP12 (=TYROBP) deficiency caused osteopetrosis associated with increased bone mass, failed osteoclast development and/or impaired bone remodeling [24]. Noteworthy, the number of multinucleated osteoclasts per unit trabecular surface was comparable to that of control mice. Thus, an impairment of function rather than reduction in number of osteoclasts was likely the reason of reduced bone resorption. Interestingly, in-vitro bone marrow cultures in this study showed that induction of osteoclasts was significantly hampered in DAP12$^{-/-}$ mice compared to wild type. Further, the mutant osteoclasts were devoid of an actin-sealing ring and had a reduced ability to form resorption pits on dentin surfaces. This partly links the NHD to osteopetrosis, in which the dysfunction of osteoclasts results in excessively dense, yet brittle bones.

Considering the characteristics of the transiliac bone biopsy sample of our patient with mutations in the *TYROBP* gene, the increased cortical width, the abnormal changes in bone lamellae orientation and especially the significantly elevated bone matrix mineralization would be compatible with dysfunctional osteoclasts. In childhood and adolescence, the two cortical plates of the iliac crest bone have to make a centrifugal drift during growth. At the external cortex, this is accomplished by new bone deposition on the periosteal side (osteoblast activity), coupled with simultaneous trabecularization (osteoclast activity) of the endosteal side. At the internal cortex bone resorption occurs by osteoclasts at periosteal side and new bone deposition by osteoblasts at the endosteal side [9,25]. Thus, disturbances in osteoclast function would lead to thicker cortices at this specific skeletal site. Recently, such a broadening of the cortical plates due to the reduction of osteoclast resorption activity by bisphosphonate treatment was well demonstrated in a case of osteogenesis imperfecta type V [26].

A further indication of disturbed osteoclast function arose from the abnormal highly disordered lamellar structure within the trabecular motifs in our propositus. This kind of abnormality strongly resembles cases with pycnodysostosis [27], a condition resulting from mutations in the cathepsin K gene, a lysosomal cysteine protease highly expressed in osteoclasts and crucial for the degradation of organic matrix in the resorption lacunae. This type of dysfunction of osteoclasts leads to high bone mass, accompanied by increased bone fragility. The abnormal lamellar arrangement is thought to contribute to the reduced bone strength evident in these patients. We would like to point out that the abnormal lamellar bone structure seen in our propositus's bone sample is likely the result of remnants from earlier intense (re)modeling activities during adolescence, before the bone turnover declined to the abnormally low values shown by histomorphometry.

The shift of the bone mineralization density distribution curve toward higher mineral content in our propositus compared to normative reference [15], consistent with the observed increase in bone mineral density due to antiresorptive treatment [28], might be a further compelling indication of osteoclastic dysfunction. It has to be emphasized that the BMDD may be considered as a kind of fingerprint of bone matrix mineralization [13,29]. It reflects the history of bone cells activity, such as conditions of low and high bone turnover rates as well as changes/abnormalities in the time course of mineral accumulation in newly formed bone. Bone at the tissue/material level is composed by bone packets or bone structural units (BSU), formed by osteoblasts during one bone formation cycle. The mineral content of these BSUs is increasing with time, thus BSUs with young tissue age have the lowest and BSUs with old tissue age have the highest mineral content. Consequently, if the bone turnover is markedly reduced as it is the case in our propositus, the bone packets have in average more time to mineralize before they get resorbed by the osteoclasts during the remodeling process. These results in an elevated bone matrix mineralization compared to individuals with normal bone turnover rates. Most likely both the low osteoclast number and their disturbed ability to resorb bone contribute to the observed bone hypermineralization in our propositus. The osteoblasts, which belong to the mesenchymal cells lineage, seem to be unaffected by the *TYROBP* gene mutation, as they consistently produced collagen, without any alterations in the collagen cross-links pattern.

In summary, the discrete cystic-like bone lesions as observed in carpals, tarsals and the metaphyses of the long bones in our patient were associated with two mutations in the *TYROBP* gene causing the NHD. Additionally, the bone biopsy findings revealed abnormalities in histomorphometric and mineralization characteristics. These novel bone tissue/material data from a patient with NHD are consistent with impaired osteoclast function due to mutations in *TYROBP* gene resulting in material/mineralization abnormalities. In addition to the local cystic-like bone lesions in the long bones, these global skeletal abnormalities contribute to bone brittleness and fragility.

Acknowledgment

We wish to thank the family members for their willing participation and cooperation with this study. We thank Sonja Lueger, Petra Keplinger and Phaedra Messmer from Ludwig Boltzmann Institute of Osteology for sample preparation, histomorphometry and qBEI measurements.

This work was financially supported by the by the AUVA (research funds of the Austrian workers compensation board) and the WGKK (Viennese sickness insurance funds).

Disclosures

None.

References

[1] T. Nasu, Y. Tsukahara, K. Terayama, N. Mamiya, An autopsy case of "membranocystic" lipodystrophy with myelo-osteopathy of long bones and leucodystrophy of the brain Tokyo, 59th Tokyo Meeting of Pathology, 1970.

[2] T. Nasu, Y. Tsukahara, K. Terayama, N. Mamiya, A lipid metabolic disease – "membranous lipodystrophy" – an autopsy case demonstrating numerous peculiar membrane-structures composed of compound lipid in bone and bone marrow and varios adipose tissues, Acta Pathol. Jpn. 23 (1973) 539–558.

[3] H.P.A. Hakola, O.H. Jarvi, P. Sourander, Osteodysplasia polycystica hereditaria combined with sclerosing leucoencephalopathy, a new entity of the dementia praesenilis group, Acta Neurol. Scand. 46 (Suppl. 43) (1970) 79–80.

[4] M.M. Bianchin, H.M. Capella, D.L. Chaves, Nasu-Hakola disease (polycystic Lipomembranous Osteodysplasia with Sclerosing leukoencephalopathy—PLOSL): a dementia associated with bone cystic lesions. From clinical to genetic and molecular aspects, Cell. Mol. Neurobiol. 24 (1) (2004) 1–24.

[5] J. Paloneva, M. Kestila, J. Wu, A. Salminen, T. Bohling, V. Ruotsalainen, P. Hakola, A.B. Bakker, J.H. Phillips, P. Pekkarinen, L.L. Lanier, T. Timonen, L. Peltonen, Loss-of-function mutations in TYROBP (DAP12) result in a presenile dementia with bone cysts, Nat. Genet. 25 (2000) 357–361.

[6] J. Paloneva, T. Manninen, G. Christman, K. Hovanes, J. Mandelin, R. Adolfsson, M. Bianchin, T. Bird, R. Miranda, A. Salmaggi, L. Tranebjaerg, Y. Kontinnen, L. Peltonen, Mutation in tw genes encodi9ng for different subunits of a receptor signalling complex result in an identical disease phenotype, Am. J. Hum. Gent. 71 (2002) 656–662.

[7] P. Fratzl, H. Gupta, E. Paschalis, P. Roschger, Structure and mechanical quality of the collagen-mineral nano-composite in bone, J. Mater. Chem. 14 (2004) 2115–2123, https://doi.org/10.1039/B402005G.

[8] L. Palenzuela, C. Vives-Bauza, I. Fernandez-Cadenas, A. Meseguer, N. Font, E. Sarret, S. Schwartz, A.L. Andreu, Familial expansile osteolysis in a large Spanish kindred resulting from an insertion mutation in the TNFRSF11A gene, J. Med. Genet. 39 (2002) e67.

[9] F. Rauch, R. Travers, F.H. Glorieux, Cellular activity on the seven surfaces of iliac bone: a histomorphometric study in children and adolescents, J. Bone Miner. Res. 21 (4) (2006) 513–519.

[10] David W. Dempster, Juliet E. Compston, Marc K. Drezner, Francis H. Glorieux, John A. Kanis, Hartmut Malluche, Pierre J. Meunier, Susan M. Ott, Robert R. Recker, A. Michael Parfitt, Standardized nomenclature, symbols, and units for bone histomorphometry: a 2012 update of the report of the ASBMR histomorphometry nomenclature committee, J. Bone Miner. Res. 28 (2013) 2–17.

[11] C.A. Schneider, W.S. Rasband, K.W. Eliceiri, NIH image to ImageJ: 25 years of image analysis, Nat. Methods 9 (2012) 671–675.

[12] M.T.A. Rehman, J.A. Hoyland, J. Denton, A.J. Freemont, Age related histomorphometric changes in bone in British men and women, J. Clin. Pathol. 47 (1994) 529–534.

[13] P. Roschger, E.P. Paschalis, P. Fratzl, Bone mineralization density distribution in health and disease, Bone 42 (3) (2008) 456–466.

[14] P. Roschger, P. Fratz, J. Eschberger, K. Klaushofer, Validation of quantitative backscattered electron imaging for the measurement of mineral density distribution in human bone biopsies, Bone 23 (1998) 319–326.

[15] P. Roschger, H.S. Gupta, A. Berzlanovich, G. Ittner, D.W. Dempster, P. Fratzl, F. Cosman, M. Parisien, R. Lindsay, J.W. Nieves, K. Klaushofer, Constant mineralization density distribution in cancellous human bone, Bone 32 (2003) 316–323.

[16] E.P. Paschalis, Fourier transform infrared imaging of bone, Methods Mol. Biol. 816 (2012) 517–525.

[17] S. Gamsjaeger, R. Mendelsohn, A.L. Boskey, S. Gourion-Arsiquaud, K. Klaushofer, E.P. Paschalis, Vibrational spectroscopic imaging for the evaluation of matrix and mineral chemistry, Curr. Osteoporos. Rep. 12 (2014) 454–464.

[18] E.P. Paschalis, S. Gamsjaeger, K. Klaushofer, Vibrational spectroscopic techniques to assess bone quality, Osteoporos. Int. 28 (8) (2017) 2275–2291.

[19] E.P. Paschalis, K. Verdelis, S.B. Doty, A.L. Boskey, R. Mendelsohn, M. Yamauchi, Spectroscopic characterization of collagen cross-links in bone, J. Bone Miner. Res. 16 (10) (2001) 1821–1828.

[20] E.P. Paschalis, D.N. Tatakis, S. Robins, P. Fratzl, I. Manjubala, R. Zoehrer, S. Gamsjaeger, B. Buchinger, A. Roschger, R. Phipps, A.L. Boskey, E. Dall'Ara, P. Varga, P. Zysset, K. Klaushofer, P. Roschger, Lathyrism-induced alterations in collagen cross-links influence the mechanical properties of bone material without affecting the mineral, Bone 49 (6) (2011) 1232–1241.

[21] E.P. Paschalis, S. Gamsjaeger, D.N. Tatakis, N. Hassler, S.P. Robins, K. Klaushofer, Fourier transform infrared spectroscopic characterization of mineralizing type I collagen enzymatic trivalent cross-links, Calcif. Tissue Int. 96 (1) (2015) 18–29.

[22] B.M. Misof, D.W. Dempster, Zhou Hua, P. Roschger, N. Fratzl-Zelman, P. Fratzl, S.J. Silverberg, E. Shane, A. Cohen, E. Stein, T.L. Nickolas, R.R. Recker, J. Lappe, J.P. Bilezikian, K. Klaushofer, Relationship of bone mineralization density distribution (BMDD) in cortical and cancellous bone within the iliac crest of healthy premenopausal women, Calcif. Tissue Int. 95 (2014) 332–339.

[23] S.P. Robins, Biochemistry and functional significance of collagen cross-linking, Biochem. Soc. Trans. 35 (2007) 849–852.

[24] T. Kaifu, J. Nakahara, M. Inui, Osteopetrosis and thalamic hypomeelinois with snaptic degeneration in DAP12-deficient mice, J. Clin. Invest. 111 (2003) 323–332.

[25] N. Fratzl-Zelman, P. Roschger, B.M. Misof, et al., Normative data on mineralization density distribution in iliac bone biopsies of children, adolescents and young adults, Bone 44 (6) (2009) 1043–1048.

[26] Stephane Blouin, Nadja Fratzl-Zelman, Francis H. Glorieux, Paul Roschger, Klaus Klaushofer, Joan C. Marini, Frank Rauch, Hypermineralization and high OsteocyteLacunar density in osteogenesis imperfecta type V bone indicate exuberant primary bone formation, J. Bone Miner. Res. 32 (2017) 1884–1892.

[27] N. Fratzl-Zelman, A. Valenta, P. Roschger, A. Nader, B. Gelb, P. Fratzl, K. Klaushofer, Decreased bone turnover and deterioration of bone structure in two cases of pycnodysostosis, J. Clin. Endocrinol. Metab. 89 (2004) 1538–1547.

[28] Peter Fratzl, Paul Roschger, Nadja Fratzl-Zelman, Eleftherios P. Paschalis, Roger Phipps, Klaus Klaushofer, Evidence that treatment with risedronate in women with postmenopausal osteoporosis affects bone mineralization and bone volume, Calcif. Tissue Int. 81 (2007) 73–80.

[29] D. Ruffoni, P. Fratzl, P. Roschger, R. Phipps, K. Klaushofer, R. Weinkamer, Effect of temporal changes in bone turnover on the bone mineralization density distribution: a computer simulation study, J. Bone Miner. Res. 23 (12) (2008) 1905–1914, https://doi.org/10.1359/jbmr.080711.

[30] P. Kumar, S. Henikoff, P.C. Ng, Predicting the effects of coding non-synonymous variants on protein function using the SIFT algorithm, Nat Protoc. 4 (2009) 1073–1081.

[31] I.A. Adzhubei, S. Schmidt, L. Peshkin, V.E. Ramensky, A. Gerasimova, P. Bork, A.S. Kondrashov, S.R. Sunyaev, A method and server for predicting damaging missense mutations, Nat. Methods 7 (2010) 248–249.

[32] R. Grantham, Amino acid difference formula to help explain protein evolution, Science 185 (4154) (1974) 862–864.

[33] K.A. Jagadeesh, A.M. Wenger, M.J. Berger, H. Guturu, P.D. Stenson, D.N. Cooper, J.A. Bernstein, G. Bejerano, M-CAP eliminates a majority of variants of uncertain significance in clinical exomes at high sensitivity, Nat. Genet. 48 (2016) 1581–1586.

[34] K.S. Pollard, M.J. Hubisz, K.R. Rosenbloom, A. Siepel, Detection of nonneutral substitution rates on mammalian phylogenies, Genome Res 20 (2010) 110–121.